Contents lists available at ScienceDirect

Molecular Phylogenetics and Evolution

journal homepage: www.elsevier.com

When did anoles diverge? An analysis of multiple dating strategies

Cristian Román-Palacios[a, b, *], Jose Tavera[a], María del Rosario Castañeda[a, c]

[a] Departamento de Biología, Facultad de Ciencias Exactas y Naturales, Universidad del Valle, A. A. 25360 Cali, Valle del Cauca, Colombia
[b] Department of Ecology and Evolutionary Biology, University of Arizona, Tucson, AZ 85721-0088, USA
[c] Departamento de Ciencias Biológicas, Facultad de Ciencias Naturales, Universidad Icesi, Calle 18 No. 122-135, Cali, Colombia

ARTICLE INFO

Keywords:
Anolis
Chronograms
Divergence dating
Fossil dating
Malpelo anole
Rate-based calibration

ABSTRACT

Whereas most of the studies that discuss the evolutionary divergence of *Anolis* lizards have dated the clade's crown group in between 31 and 64 Ma, a single study has recovered a significantly older age for the same node (87 Ma). These differences also entail notable consequences on the preferred biogeographical hypothesis for the whole clade. Here we analyze a total of seven dating strategies by combining three calibration sources in independent BEAST runs to infer the most probable divergence timing for anole lizards (a mitochondrial rate for ND2 gene, the *Anolis dominicanus* fossil, and a group of fossils assigned to the Priscagamines, Iguanines, and *Idontosaurus* clades). Based on the estimated timing, we also addressed whether chronograms differ the most in deeper or shallower nodes by exploring the trend in the standard deviation of mean ages between chronograms across time. Next, we focus on the pattern for a single shallow node by hypothesizing the biogeography of the island-endemic Malpelo anole (*Anolis agassizi*), and evaluating the temporal congruence between the species' divergence and the island geology. The estimated set of ages suggests that anoles most likely diverged 72 Ma (71–73 Ma), with the crown group established around 58 Ma (51–65 Ma). Dispersal is therefore supported as the major driver in the biogeography of the group (and in Caribbean lineages in particular). Our analyses also indicated that (1) rate-based analyses pulled dates toward younger ages, (2) the differences in node ages between chronograms decrease towards the tips regardless of the position of the constrained node, and that (3) the estimated age for deep nodes (e.g. *Anolis* stem) is highly influenced when deep nodes are also constrained. The latter two results imply that the estimated age for shallower nodes is largely unaffected by the used temporal constraint. The congruence of all chronograms for the Malpelo anole also support this finding. *Anolis agassizi* was found to have diverged before the emergence of Malpelo island in each analysis (anole: 19–31 Ma vs. Malpelo island: 16–17 Ma). We recommend when performing absolute dating analyses to first test for sequence saturation in the analyzed dataset (especially when calibrations are based on molecular rates). Our study also points out the importance of using of multiple node constraints, especially when placed deeply in the tree, for fossil–based divergence dating analyses.

1. Introduction

With more than 400 species, *Anolis* lizards are among the most diverse vertebrate groups (Uetz and Hošek,2016). Despite anoles playing a central role in our understanding of several evolutionary processes such as diversification dynamics (e.g. Kolbe et al., 2011), trait evolution (e.g. Mahler et al., 2013), ecological opportunity (e.g. Algar et al., 2016), and biogeography (e.g. Campbell-Staton et al., 2012), the clades' divergence timing is still under debate (Townsend et al., 2011; Nicholson et al., 2012; Castañeda et al., 2014; Prates et al., 2015; Poe et al., 2017). Here we primarily discuss *Anolis* divergence timing by comparing the estimated ages of chronograms calibrated based on a set of well-supported divergence evidences (see below; Table 1).

To date, multiple studies have estimated the stem age of *Anolis* lizards. However, there is considerable variation among studies based different methods and data sources (e.g. fossils and molecular clocks). Initially, Townsend et al. (2011) used a concatenated dataset of 29 protein-coding genes to estimate the stem age of *Anolis* in 65.5 Ma (50–70 Ma; anole spp. = 1). Later, Daza et al. (2012), using an updated morphological dataset from Conrad (2008), estimated the same node in ~ 50 Ma (anole species = 1). Next, Blankers et al. (2012) used the

* Corresponding author at: Departamento de Biología, Facultad de Ciencias Exactas y Naturales, Universidad del Valle, A. A. 25360 Cali, Valle del Cauca, Colombia.
Email address: cromanpa94@email.arizona.edu (C. Román-Palacios)

https://doi.org/10.1016/j.ympev.2018.06.012
Received 4 December 2017; Received in revised form 27 April 2018; Accepted 6 June 2018
Available online xxx
1055-7903/

Table 1
Description of calibration sources used in dating analyses with details on the specified parameters for each. For both fossil calibrations, mean and standard deviation corresponded to 1.

Code	Calibration source	Priors on age	95% Probability density (based on BEAST)	Description	References
F1	*Anolis* fossil	Lognormal Offset = 17	17.1–21.3	This node comprises all three described *A. dominicanus* amber fossils. The phylogenetic position has been widely discussed and recently assigned to the *chlorocyanus* series (minimum age)	De Queiroz et al. (1998); Sherratt et al. (2015); Poe et al. (2017)
F2	Pleurodonta (Iguania) fossils	Lognormal Offset = 70	71.0–74.3	Includes the fossils assigned to Priscagamines, Iguanines, and *Isodontosaurus*. Their position was based on phylogenetic analyses. These fossils constraints the minimum age of the stem group of Pleurodonta clade (Iguania)	Conrad (2008); Mulcahy et al. (2012); Poe et al. (2017)
Rate	Mitochondrial evolutionary rate	0.65%/lineage/Ma	–	Several time-calibrated phylogenies in *Anolis* are based on the evolutionary rate for certain mitochondrial genes. We used the rate estimated from *Laudakia* (Agamidae)	Macey et al. (1998, 1999)

dataset presented by Townsend et al. (2011) in addition of a protein-coding mitochondrial gene (ND2), to estimate the *Anolis* stem age in about 70 Ma (~61–82 Ma; anole species = 3). Mulcahy et al. (2012), provided two different ages for the *Anolis* stem clade based on 25 protein-coding loci: 25–75 Ma as estimated by BEAST dating, and ~80 Ma using a penalized likelihood method (anole species = 1). Nicholson et al. (2012), based on two protein-coding and six non-protein genes, found one of the oldest estimates for the stem-clade *Anolis* (ca. 95 Ma; anole species = 189). Prates et al. (2015), using seven protein-coding genes and one RNA region, estimated the *Anolis* stem age in about 82 Ma (71–99 Ma; anole species = 33). More recently, Poe et al. (2017), using the most comprehensive species-level phylogeny for anoles based on a combined dataset of morphological and three protein-coding genes, dated the stem age of the group in ca. 71 Ma (69–72 Ma; anole species = 379). In contrast, fewer papers have provided age estimates for the *Anolis* crown group. Blankers et al. (2012) estimated this node in about 38 Ma (~31–47 Ma), Nicholson et al. (2012) in ~87 Ma (no range provided by the authors), Prates et al. (2015) in 49 Ma (38–63 Ma), and Poe et al. (2017) estimated the same node in about 51 Ma (46.3–64.4 Ma).

The estimated age of the *Anolis* crown group has a significant impact on interpreting the biogeography of the clade (especially Caribbean lineages; Crother and Guyer, 1996; Hedges, 1996; Hedges et al., 1994). Two major hypotheses have been proposed to explain the current distribution of Caribbean *Anolis*. Vicariance–driven biogeography is supported when older ages are inferred for the crown group (e.g. Guyer and Savage, 1986). In contrast, younger ages imply dispersal as a major biogeographical driver in anoles (e.g. Hedges et al., 1992). Even though most analyses have supported a predominantly dispersal–driven biogeography in Caribbean anoles (e.g. Hedges et al., 1992; Calsbeek and Smith, 2003; Poe et al., 2017), Nicholson et al. (2012) found support for a vicariance–driven scenario for the same lineages, which was initially proposed by Guyer and Savage (1986).

Previous studies have suggested that the age estimates presented in Nicholson et al. (2012) are flawed. We highlight two lines of evidence that have challenged Nicholson's et al. (2012) results. First, several authors have agreed on the low likelihood of hypotheses based on vicariance to explain the historical patterns of Antillean anoles (e.g. crown–age estimations suggest that anoles' lineages are younger than the island system; see discussion in Poe et al., 2017 and references therein). Secondly, the position of one of the fossils used by Nicholson et al. (i.e. *Anolis electrum*) is still unsupported within the anoles phylogeny (Castañeda et al., 2014; Poe et al., 2017), and its placement seems to be pulling node ages backwards towards older dates.

Here, we primary aim to address when anoles diverged. We follow a methodological approach that can be easily extended to other taxonomic groups with debatable and problematic divergence date estimates. First, we used three different calibration sources to estimate divergence times across the tree: the ND2 mitochondrial rate, the age of the *Anolis dominicanus* fossil, and multiple fossils to calibrate the Pleurodonta crown group. Each calibration source was analyzed independently, and in all possible combinations. We compared the estimated likelihood values of the seven chronograms using Bayesian two-sample t-tests and Bayes factors to answer: Are chronograms based on multiple evidence (i.e., combinations of calibration sources) better explanations of the anole evolutionary timing than divergence hypotheses based on a single calibration sources?

Second, we discuss how the use of different time–estimation strategies might lead to different date estimates across the phylogeny. To date, most discussions about the timing of *Anolis* diversification have focused on its basal divergence (e.g. stem or crown groups). However, it is widely known that node ages are highly variable when different constraints are applied to molecular clocks (e.g. molecular rates vs node constraints; Mello and Schrago, 2014; van Tuinen, 2015). We addressed whether chronograms differed most in deeper or shallower nodes by exploring the change over time in the standard deviation of node ages between chronograms. Furthermore, we analyzed the effect of the position of fossil constraints (i.e. deep or shallow in tree) regarding the variation in mean age estimates across the phylogeny to test whether lower between-chronograms variation in dates are associated to deep or shallow nodes. This topic has been rarely discussed in the literature (Mello and Schrago, 2014; Duchêne et al., 2014).

Third, we focused on the pattern between chronograms for a single shallow node. We compared the estimated divergence of *Anolis agassizi* to the emergence of the island to which this species is endemic to (Malpelo island). This oceanic island is located 380 km off the Pacific coast of Colombia and probably emerged 16–17 Ma (Hoernle et al., 2002). We suggest that both the degree of isolation and the known age of this oceanic island provide an ideal scenario to evaluate the congruence between biogeography and evolutionary timing for this island-endemic anole.

2. Methods

2.1. Phylogenetics

Our analyses were based on 73 taxa comprising 68 *Anolis* species from the major taxonomic series (see Williams, 1976a, 1976b). We included five outgroup species representing the Pleurodontid genera *Enyalioides*, *Polychrus*, *Pristidactylus*, *Oplurus*, and *Urostrophus*. Taxo-

nomic sampling for both ingroup (see Jackman et al., 1999, Castañeda and de Queiroz, 2011) and outgroup follow previous studies (Conrad, 2008; Townsend et al., 2011). The taxonomic sampling used here aims to maximize the coverage across major anole series without sampling every single species in the anole phylogeny.

We sampled both fast– and slow–evolving genes to estimate the phylogenetic relationships and divergence dates among anoles. Our molecular sampling comprises the mitochondrial NADH dehydrogenase subunit II (ND2, c. 1500 bp), the five-adjacent transfer-RNA ($tRNA^{Trp}$, $tRNA^{Ala}$, $tRNA^{Asn}$, $tRNA^{Cys}$, $tRNA^{Tyr}$), the origin of light-strand replication (O_L), and a fragment of the cytochrome oxidase subunit I (COI, c. 650 bp), and the nuclear recombination-activating gene (RAG-1, c. 2800 bp). A list of species and accession numbers is provided in Table A.1.

Protein coding genes (ND2, COI and RAG-1) were aligned in MUSCLE v.3.8 (Edgar, 2004) using a translation–based alignment with 10 iterations and setting all other parameters as default. The resulting alignment was visually inspected to ensure the correct protein–coding reading frame. The tRNA region was aligned considering its structural complexity and following the secondary structure model proposed by Kumazawa and Nishida (1993). Models of DNA sequence evolution and partitioning schemes were selected using PartitionFinder v.1.1.0 (Lanfear et al., 2012) based on a Bayesian Information Criteria (BIC) and a greedy algorithm. We set codon–based partitions for protein-coding genes in PartitionFinder analyses, and allow unlinked branch lengths between partitions.

The final concatenated alignment had a length of 4710 bp. The following nucleotide positions were excluded from the concatenated alignment due to the ingroup–outgroup ambiguity (positions are relative to *Urostrophus gallardoi*): 19–27, 46–49, 56–64, 75–77, 92–98, 102–106, 129–133, 146–148, 162–168, 175–181, 203–210, 224, 234, 236–255, 264–267, 279–294, 302–307, 327, 336–337, 344–351, 364–370, 378–381, and 403–409.

2.2. Sequence saturation

Gene saturation is known to affect molecular dating analyses by biasing the estimated genetic distances (see Wilke et al., 2009; Schwartz and Mueller, 2010; Magallón et al., 2013). Some authors have suggested that saturated genes can either (1) pull older nodes towards younger ages (Marshall et al., 2016), or (2) overestimate the age of younger nodes (Phillips, 2009; Zheng et al., 2011). This effect is thought to be stronger when absolute dates are exclusively based on molecular rates (e.g. the mitochondrial rate used here; Weir and Schluter, 2008; Magallón et al., 2013). Gene saturation was tested for all genes (COI, ND2, RAG1, and all tRNAs combined), each codon position for protein genes (COI, ND2, and RAG1), and each PartitionFinder subset in the best-fitting partitioning scheme (see above; Table A.2). We inspected the relationship between uncorrected distances (*p*-distances) and corrected distances based on HKY model. Under this approach, saturated gene regions are shown as curved lines. Conversely, non-saturated regions are expected to recover a linear relationship between *p* and corrected distances.

2.3. Divergence dating analyses

We used three different calibration sources to estimate divergence times in *Anolis* (Table 1; Fig. A.1). First, we used a per lineage molecular clock average rate of 0.65% change/lineage/Ma (i.e. 1.3% divergence/Ma) derived from ND2, $tRNA^{Trp}$ and $tRNA^{Ala}$ (Macey et al., 1998, 1999). Second, we used the fossil species *Anolis dominicanus* to calibrate the crown age of the *chlorocyanus* series (de Queiroz et al., 1998; Sherratt et al., 2015; Poe et al., 2017; Table 1; Fig. A.1). Lastly, we used a group of fossils assigned to the Priscagamines, Iguanines and *Isodontosaurus* clades for constraining the age of the Pleurodonta crown group (Mulcahy et al., 2012, Poe et al., 2017; Table 1; Fig. A.1). We applied a total of seven dating strategies, resulting from analyzing each calibration source independently and in all possible combinations: (1) Rate, (2) *Anolis dominicanus* fossil (F1), (3) Iguania fossils (F2), (4) Rate + F1, (5) Rate + F2, (6) F1 + F2, and (7) Rate + F1 + F2.

The phylogenetic relationships and absolute dating for *Anolis* were simultaneously inferred using BEAST v.2.3.0 (Bouckaert et al., 2014). Partitioning strategy and evolutionary model implemented follows PartitionFinder results (Table A.2). Molecular clock partitions were unlinked between nuclear and mitochondrial genes in BEAST and all loci were linked into a single tree. We selected a Birth–Death process for the speciation prior and allowed branch lengths to be uncorrelated across the tree. For rate–based analyses (i.e. Rate, Rate + F1, Rate + F2, Rate + F1 + F2), we set a relaxed log normal clock in both nuclear and mitochondrial partitions. However, instead of estimating the rate for the later partition, we fixed its clock rate to 0.0065 (0.65%; see Table 1). For both fossil calibrations (F1, and F2), we followed Mulcahy et al. (2012) by specifying a lognormal distribution, and setting both mean and standard deviation to 1. The distribution offset for each of these fossil calibrations was set to the minimum fossil date (see Table 1).

For each dating analysis, two independent runs consisting of 20 million generations with parameters logged every 2,000 generations were analyzed in the CIPRES cluster (Miller et al., 2011). BEAST XML files provided in Supplementary File 1. Both log and tree files resulting from each independent run were merged after discarding the first 25% generations as burn-in with LogCombiner v.2.3.0. A maximum clade credibility (MCC) tree based on mean branch length was obtained in TreeAnnotator v.2.3.0. We assessed convergence of the runs using Tracer v.1.6 (Rambaut et al., 2007) by considering effective sample size (ESS) on likelihood over 200 as indicator.

2.4. Chronogram comparison

We calculated the mean age and standard deviation associated to every node based on the seven BEAST MCC chronograms (all shared the same topology, see results). We plotted this relationship to visually examine the variation in the estimated ages among chronograms across time. Then, we used two statistical approaches to statistically compare the hypotheses. First, we compared posterior distribution of likelihood values between chronograms using paired Bayesian two-sample t-tests (Rouder et al., 2009). These analyses were performed using the ttestBF function implemented in the BayesFactor R package (Morey et al., 2015). Statistical significance of these comparisons was assessed based on two-tailed tests. Next, we calculated the pairwise Bayes Factors (BF) values between BEAST chronogram runs using Tracer v.1.6 (see Andújar et al., 2014). These analyses were based on the post-burning sampling fraction, and the error in the harmonic mean estimator during BF calculations was calculated using 1000 bootstrap replicates. For these analyses, pairwise BF (estimated as $2\log_e xB_{10}$) larger than 10 were indicative of strong support of one chronogram over another (Kass and Raftery, 1995).

3. Results

3.1. Sequence saturation

Sequence saturation varied among the analyzed gene regions and partitions. We found no saturation in the RAG-1 and tRNA genes (Fig. A.2). However, we did find saturation in the ND2 and COI genes. Several codon positions were saturated within the same protein-coding gene (Fig. A.3). For instance, codon positions 1 and 3 were found satu-

rated in COI. All codon positions in ND2 were saturated, and only codon position 3 was saturated in RAG1 gene. Among the partitioning schemes identified by PartitionFinder (see Table A.2), only a single scheme (i.e. Scheme 2) containing COI codon position 2 and all RAG1 positions, was found to be unsaturated (Fig. A.4).

3.2. Divergence times

Identical topologies were inferred by the seven BEAST chronograms suggesting that calibration strategies placed no effect on the resulting topology (Fig. 1). The monophyly of *Anolis* is strongly supported (Posterior Probability (PP) = 1), and the relationships within the clade were fully resolved, strongly supported (trees provided in Supplementary File 2), and largely congruent with previously published phylogenies (Fig. 1; Castañeda and de Queiroz, 2011; Nicholson et al., 2012; Poe et al., 2017).

Our time–calibrated phylogenies dated the stem clade of *Anolis* in between 61 Ma (Rate calibration strategy; 52.77–70.34 Ma) and 72 Ma (F1 + F2 calibration strategy; 71.03–73.62 Ma; Table 2; Fig. 2A). In all cases, the 95% High Probability Density (95% HPD) intervals partially overlapped between chronograms, indicating agreement between dating strategies for the estimated age at the same node. Calibration strategies containing F2 fossil showed the smallest variation in the estimated age for the stem group (e.g. F2, F1 + F2, F2 + Rate, F1 + F2 + Rate; Fig. 2A). All dating strategies inferred a Paleogene divergence for the crown group between 51 Ma (Rate calibration strategy; 45.77–56.76 Ma; Table 2) and 59 Ma (F2 calibration strategy; 52.28–67.29 Ma: Fig. 2B).

Overall, for both stem and crown groups, rate-based estimations inferred the youngest ages across all chronograms. Stem age estimates seemed to be heavily influenced by the F2 calibration, resulting in narrow 95% HPD intervals, probably because this node-based constraint was also applied deep in the tree (i.e. Pleurodonta crown; Fig. 2A). Interestingly, this pattern is not present in the crown age, where most of the chronograms suggested a set of largely similar dates with large 95% HPD intervals (Fig. 2B). Among all the dating strategies, the F1 inferred the largest 95% HPD intervals for both the stem and crown groups (Fig. 2).

Results indicated that *Anolis agassizi* and its sister species, *A. insignis*, diverged during the Oligocene, between 22 Ma (Rate calibration strategy; 17.58–27.05) and 26 Ma (F2 calibration strategy; 19.39–31.88 Ma; Table 3). Age estimates were very close to each other across chronograms, suggesting that dating evidences placed no effect on the estimated age for this shallow node (Table 3; Fig. 3). In all cases the estimated divergence age for *A. agassizi* occurs prior to the emergence of Malpelo island.

3.3. Chronogram comparison

The relationship between the standard deviation of age among chronograms and node age is shown in Fig. 4. We found that the difference between chronograms in mean age decreases towards younger nodes suggesting that the difference between chronograms is smaller in shallower nodes, and larger in deeper nodes (e.g. *Anolis* crown vs *A. agassizi* divergence). We found that while the standard deviation of node age reaches $\sigma = 5.29$ Ma at the root of the tree (mean date = ~67 Ma), it decreases to less than $\sigma = 1$ in nodes that are younger to 14 Ma (see Fig. 4). This suggests that the difference between ages is more than five times smaller in shallower nodes, and that the estimated age for shallower nodes is hardly affected by the analyzed dating strategy (Fig. 4). These results were not influenced by the position of the fossil constraint given that the closeness of the constrained nodes seems to not place any effect on the estimated age. For instance, chronograms that were constrained using F1 or F2, consistently recovered the same pattern across the evaluated nodes (i.e. estimated crown and stem ages, and divergence between *A. agassizi* and *A. insignis*). However, F1-based estimated ages were consistently younger than other chronograms that included the F2 constraint (Fig. 2). When these two strategies were combined, the estimated ages across nodes were always closer to the age of the F2 constraint, than to the F1-based chronogram.

Despite dating strategies being found to be highly similar in terms of the estimated ages across the phylogeny (Fig. 1), we found statistical differences in likelihood values between F1 + F2 chronogram (a lower score) and all other calibration strategies (Table 4; $p < 0.05$), implying that the combination of these two fossils outperforms the fit of each fossil used independently (F1 or F2 strategies), and of all evidences combined (F1 + F2 + Rate). Bayes factors largely agreed with results based on Bayesian two-sample t-tests (BF > 44 for all pairwise comparisons made with F1 + F2; Table 5).

4. Discussion

Here, we compared divergence time estimations for *Anolis* lizards based on multiple calibration sources. This set of temporal constraints has been previously used separately in other studies (e.g. Macey et al., 1999; Townsend et al., 2011; Mulcahy et al., 2012; Poe et al., 2017), but ours is the first analysis in which all evidence (i.e. molecular, and fossil calibrations) is compared using the same dataset.

4.1. Evolutionary timing and biogeography of Anolis

According to the favored dating strategy (F1 + F2), our results strongly support an Upper Cretaceous divergence for the lineage (~72 Ma; 71.00–73.62 Ma), with the crown group established since the Paleocene (~58 Ma; 51.55–65.87 Ma). The stem age estimations closely agree with ages presented by Townsend et al. (2011; 50–70 Ma), Blankers et al. (2012; ~70 Ma), Mulcahy et al. (2012; 25–75 Ma or ~80 Ma), Poe et al. (2017; 71 Ma, 69–72 Ma), and are similar to Prates et al. (2015; 38-63 Ma). We emphasize that the F1 + F2 strategy analyzed in this paper is equivalent to the approach used by Poe et al. (2017) and Prates et al. (2015). However, ours and Poe et al.'s (2017) differ in the prior distribution used to calibrate the *chlorocyanus* series (prior distribution offset in Poe et al.: 23 Ma vs. ours: 17 Ma). On the other hand, although Prates et al. (2015) used an alternative calibration for the Pleurodonta clade (fossil: *Saichanguvel davidsoni*), both strategies are largely similar in terms of the prior information set to constraint the same node (i.e. median prior for Pleurodonta clade in Prates et al. 2015: 77.39 Ma vs ours: 70 Ma). We highlight that our dates are older than those presented by Daza et al. (2012; ~50 Ma), and much younger than those presented by Nicholson et al. (2012; ~95 Ma).

Our age estimates support dispersal as the major driver of biogeography for the radiation of modern anoles into Caribbean islands. The inferred ages for the *Anolis* crown group are consistently younger than the estimated age for the land bridge that connected North and South America that partially formed the Antillean islands (Greater Antilles Landbridge = GAL; Guyer and Savage 1986; Fig. 2B). This suggests that modern anoles reached the islands after the fragmentation of the GAL via dispersal. The alternative hypothesis, a vicariance–driven scenario, would require the *Anolis* crown group to be older than 70 Ma, an estimate only recovered by Nicholson et al. (2012). However, even if our dates for the *Anolis* crown group are remarkably similar to the formation of the early Greater Antillean Archipelago (GAA; Fig. 2B), none of the extant *Anolis* groups were already present during that time interval (i.e. 60–55 Ma; see Fig. 3). This line of evidence further support that

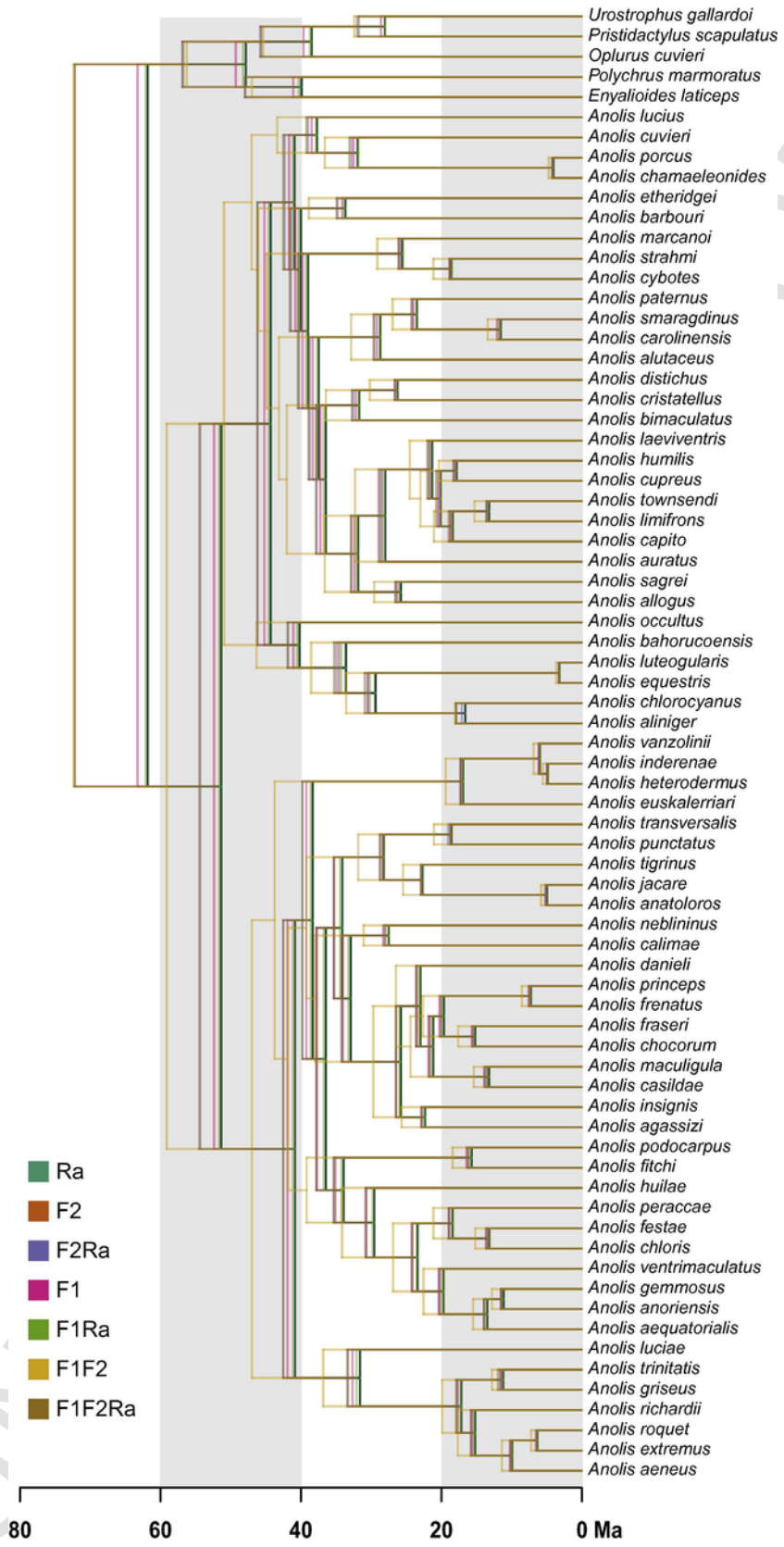

Fig. 1. Time-calibrated phylogenies for *Anolis* showing the differences in the estimated node ages across nodes. Each color represents a different chronogram (seven in total). See Tables 2 and 3, and Figs. 2 and A.1 for further details.

Table 2
Estimated ages for stem and crown *Anolis* based on the seven calibration strategies. 95% Highest Probability Density (HPD) intervals are indicated. Strategy codes are as in Table 1. Favored dating strategy (based on Bayes factors) is boldfaced (see Table 5).

Strategy	Stem group			Crown group		
	Mean	2.5%	92.5%	Mean	2.5%	92.5%
F1 + F2 + Rate	71.69	71.03	73.04	54.09	47.83	60.00
F1 + F2	**71.86**	**71.01**	**73.62**	**58.67**	**51.55**	**65.87**
F1 + Rate	61.67	53.58	70.32	51.23	45.69	57.01
F1	62.80	43.12	86.27	51.98	36.38	71.05
F2 + Rate	71.70	71.03	73.01	53.93	47.93	59.65
F2	71.94	71.03	74.00	59.37	52.28	67.29
Rate	61.35	52.77	70.34	50.97	45.77	56.75

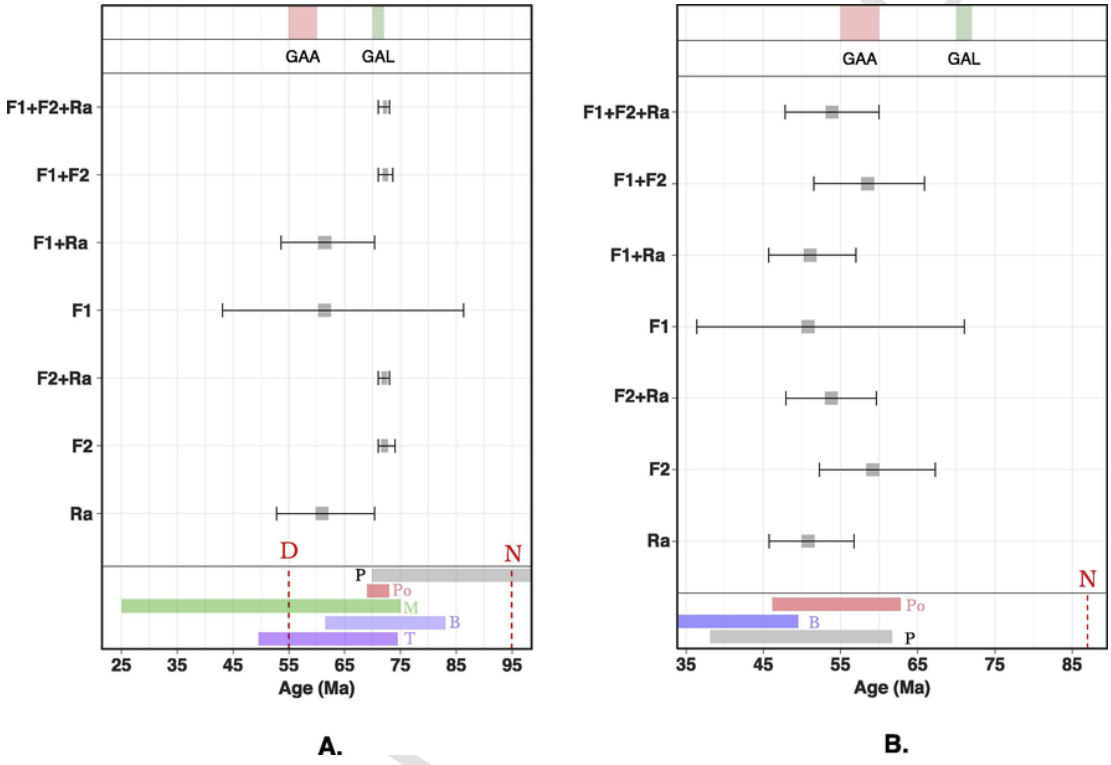

Fig. 2. Summary results for the dates estimated using seven different chronograms for (A) stem, and (B) crown groups. We provide information on previous estimates for the stem and crown ages in the bottom of figures A and B, respectively. Letter codes as follows: T: Townsend et al. (2011), D: Daza et al. (2012), B: Blankers et al. (2012), N: Nicholson et al. (2012), M: Mulcahy et al. (2012), P: Prates et al. (2015), and Po: Poe et al. (2017). At the top of the same figures, we indicate the dates for the Greater Antillean Landbridge (GAL) and the Greater Antillean Archipelago (GAA). Dates for GAL and GAA follows Nicholson et al. (2012). Bars depicting the 95% HPD for each chronogram.

Table 3
Estimated age of the divergence between *A. agassizi* and *A. insignis* based on the seven strategies. 95% Highest Probability Density intervals are shown. Strategy codes as in Table 1. Favored dating strategy (Bayes factors) is boldfaced (see Table 5).

Strategy	Mean	2.5%	97.5%
F1 + F2 + Rate	22.63	17.86	27.47
F1 + F2	**25.56**	**19.49**	**31.57**
F1 + Rate	22.26	17.29	26.49
F1	22.69	14.20	31.97
F2 + Rate	22.58	17.97	27.47
F2	25.76	19.39	31.88
Rate	22.11	17.58	27.05

speciation of these insular subclades was primarily driven by dispersal and not vicariance. We emphasize that the evolutionary timing for anoles presented by Nicholson et al. (2012) is most likely the result of the phylogenetic position of *Anolis electrum*, which is still considered uncertain (see discussion provided by Castañeda et al. 2014).

4.2. Potential biases in node age estimation

We found in our dataset that two out of three analyzed partitions were saturated. Here we briefly discuss the consequences of gene saturation for the rate–based chronograms given that this issue has been discussed elsewhere (see below). Rate chronograms differed from F2 estimated ages, but were largely similar to dates inferred using F1 strategy (see Fig. 2). Previous studies have suggested two possible outcomes when phylogenies are dated only using a rate–based evidence on alignments containing saturated genes (as in our case). First, the age of shallower nodes can be greatly overestimated (Zheng et al. 2011), or conversely, the ages in deeper nodes tends to be underestimated (Marshall et al. 2016 and references therein). After comparing all seven dating strategies, we found that the rate–based calibration tends to underestimate the age for the *Anolis* crown and stem ages (~10 Ma younger than the preferred model: F1 + F2). However, age estimates for shallower nodes were remarkably similar to fossil–based calibrated

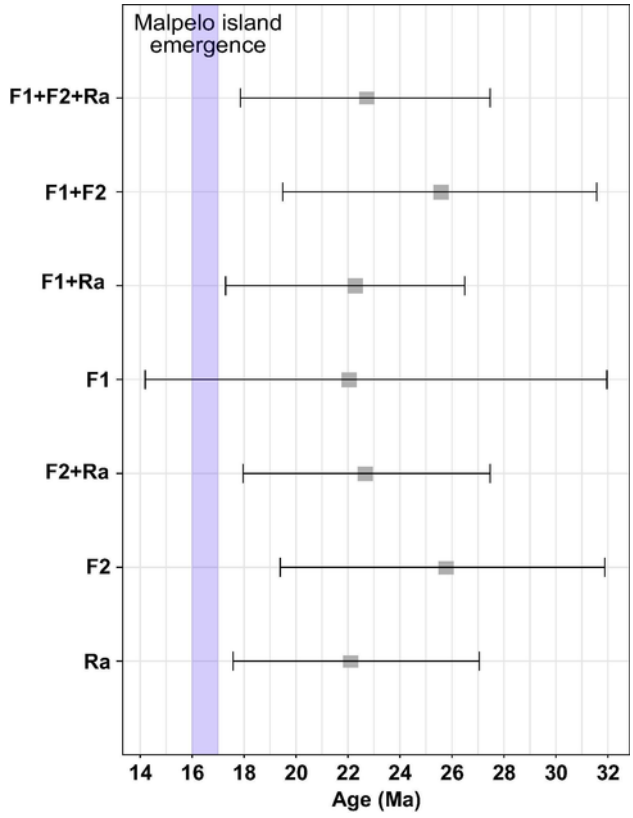

Fig. 3. Summary results for the dates estimated using seven different chronograms for the MRCA between *A. agassizi* and *A. insignis*. We indicate the emergence of Malpelo island with a blue vertical bar (16–17 Ma; see discussion). Bars depicting the 95% HPD for each chronogram.

chronograms, showing little or no saturation effect. Our results only exhibit the effect suggested by Marshall et al. (2016) who indicated that applying rate–based constraints on a dataset with saturated partitions tends to infer younger ages in deeper nodes.

4.3. On the age variation between chronograms

We found that the between–chronogram age difference decreases towards younger nodes (Fig. 3). This means that (1) ages recovered near the root are more likely to differ than near the tips for a given set of calibration strategies, and that (2) dates recovered for shallower nodes (in our case < 14 Ma) were largely congruent despite the analyzed calibration strategy. The latter result is not affected by the position of the constrained node (i.e. deep vs. shallow) with respect to the estimated node (i.e. crown, stem, or recent divergence). Here, we (1) applied a mitochondrial rate for the mitochondrial molecular clock, (2) constrained a deep node with F2, and (3) a shallow calibration with F1. We found a strong congruence between dating strategies and found no topological incompatibility between calibration sources (see Andújar et al. 2014 and references herein). In addition, we found that the estimated age for deep nodes (e.g. *Anolis* stem) is highly influenced when deep nodes are also constrained (e.g. F2 fossil). In contrast, shallow node age estimations were hardly influenced by any calibration source (e.g. *Anolis agassizi* divergence), even when shallow nodes were constrained.

Our results also reveal that shallow calibrations (e.g. F1) show larger age variation at both deep (e.g. crown and stem groups) and shallow nodes (e.g. *A. agassizi* divergence). Conversely, the use of deep calibrations (e.g. F2) results in significantly smaller confidence intervals for the estimated ages across the phylogeny. These results are in agreement with Mello and Schrago's (2014) findings that calibration constraints applied at median or deep nodes are particularly associated to smaller HPD in clade ages. In summary, our results point out the importance of combining different fossil evidenced when performing divergence dating analyses, a conclusion also reached by Duchêne et al. (2014), who suggested that an effective strategy for molecular dating should involve both multiple calibrations, combining both deep fossil and shallow fossil constraints

4.4. Biogeography and evolutionary timing of the Malpelo anole

We found that the divergence of the Malpelo anole, *Anolis agassizi* (~25 Ma) predates the island's emergence (16–17 Ma), and that this re-

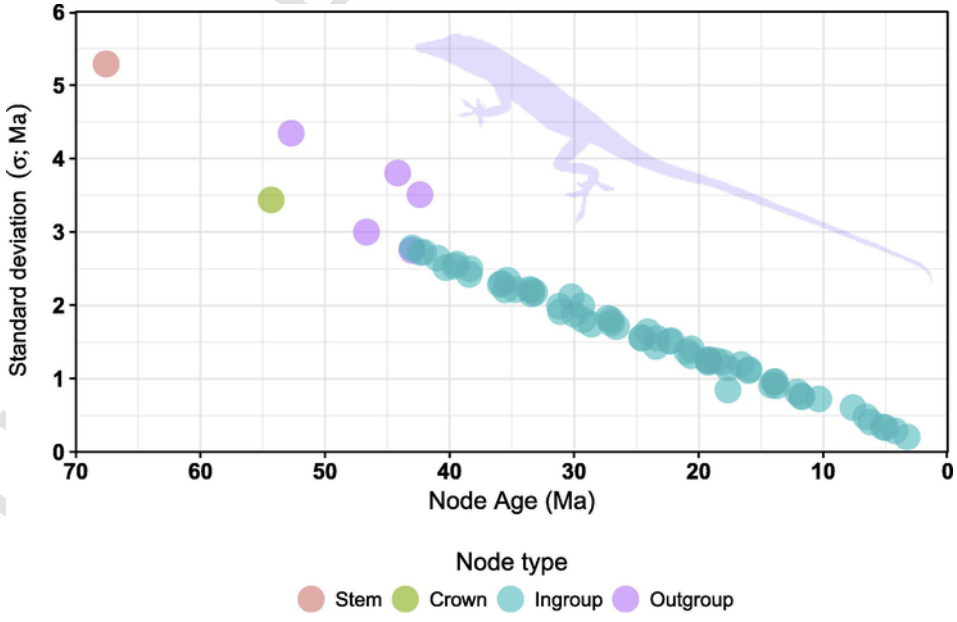

Fig. 4. Variation in the between-chronograms standard deviation of node ages across the anole phylogeny. Here we distinguish between the *Anolis* stem and crown nodes, in addition to ingroup and outgroup nodes. See Fig. A.1 for further details.

Table 4
Pairwise Bayesian t-test comparisons between the likelihood of the seven chronograms. t-statistic is indicated below the diagonal for each comparison. The associated *p*-value for each pair is indicated above the diagonal Significant statistical differences between pairs are boldfaced ($p < 0.05$). Strategy codes are as in Table 1.

Strategy	F1 + F2 + Rate	F1 + F2	F1 + Rate	F1	F2 + Rate	F2	Rate
F1 + F2 + Rate	–	**0.01**	0.87	−0.70	1.00	0.20	0.90
F1 + F2	−2.51	–	**0.03**	**0.00**	**0.02**	**0.07**	**0.01**
F1 + Rate	0.16	−2.22	–	0.64	0.88	0.30	0.78
F1	0.48	2.82	−0.47	–	0.51	0.36	0.40
F2 + Rate	0.00	−2.38	−0.16	−0.66	–	0.22	0.90
F2	1.28	−1.82	1.04	0.92	−1.22	–	0.16
Rate	−0.12	−2.59	−0.28	−0.84	−0.12	−1.40	–

Table 5
Summary results for the Bayes factors analysis. Negative values indicate row support and positive column support. Significant support of one model over another is considered when BF greater or less than 10 (boldfaced). Codes are as in Table 1.

Strategy	ln(p-model)	SE	F1 + F2 + Rate	F1 + F2	F1 + Rate	F1	F2 + Rate	F2	Rate
F1 + F2 + Rate	−55361.92	±0.45	–	**46.33**	1.95	0.20	1.31	0.45	1.12
F1 + F2	−55408.25	±1.55	**−46.33**	–	**−44.38**	**−46.13**	**−45.02**	**−45.88**	**−45.21**
F1 + Rate	−55363.87	±0.44	−1.95	**44.38**	–	−1.74	−0.63	−1.49	−0.82
F1	−55362.12	±0.46	−0.20	**46.13**	1.74	–	1.11	0.24	0.91
F2 + Rate	−55363.23	±0.56	−1.31	**45.02**	0.63	−1.11	–	−0.86	−0.19
F2	−55362.37	±0.49	−0.45	**45.88**	1.49	−0.24	0.86	–	0.67
Rate	−55363.04	±0.52	−1.12	**45.21**	0.82	−0.91	0.19	−0.67	–

sult is not dependent on the analyzed calibration strategy (see Fig. 4). All our chronograms agreed that the most recent common ancestor of *A. agassizi* and *A. insignis* occurred between 22 and 26 Ma. These dates suggesting that the divergence of Malpelo anole happened at least 5 Ma before the island's emergence (Hoernle et al. 2002; Table 3), could be interpreted in two different ways. First, we can rule out that the age of this node has been overestimated since all chronograms coincide on an early divergence (see Fig. 3). Secondly, given Malpelo has never been connected to the continent, *A. aggasizi* could only have been dispersed to the island from mainland. Two additional scenarios might be considered within this latter hypothesis. First, dispersal from mainland could have happened after speciation on mainland. Secondly, dispersal and speciation happened simultaneously. In either case, oceanic currents are hypothesized to have had played a major role in allowing *A. agassizi* to colonize Malpelo (see also Castañeda and de Queiroz, 2011), probably using the currently submerged islands via "stepping stones" for at least 5 My (M. López-Victoria pers. comm.; O'Connor et al., 2007; Bessudo et al., 2011; Jiménez et al., 2016).

However, it remains to be answered where did *Anolis agassizi* come from. Oceanic currents could also provide indirect evidence to discuss two alternatives: Central and South America. Specifically, four main oceanic currents are known to affect the coasts from South and Central America. On one hand, the strength of North Equatorial Countercurrent, the South Equatorial Current, and the Panamá current are highly influenced by El Niño Southern Oscillation (ENSO) cycles. However, historical El Niño-like cycles were strong only very recently (~3–5 Ma; Huber and Caballero, 2003; Fedorov et al., 2006), during periods that do not overlap with the divergence of *A. agassizi* or the emergence of Malpelo island. In contrast, the Colombian current, derived from the Humboldt current, which appeared >100 Ma (see Hartley et al., 2005), could have influenced the dispersal of *A. agassizi* after its divergence. However, solely based on the direction of this oceanic current (i.e. it runs along both Central and South American pacific coasts) we cannot point out which was the most likely source for the colonization for *A. agassizi*. We therefore focused on phylogenetic evidence to discuss this question. So far, the most comprehensive phylogeny of anoles (Poe et al., 2017) inferred a Central American species as sister to *A. agassizi*. This suggest that colonization from this region to Malpelo island seems more likely than from South America. In short, *A. agassizi* probably colonized Malpelo island from Central America utilizing currently submerged islands via "stepping stones" for at least 5 My.

5. Conclusions

Our analyses indicated that anoles probably diverged during the Upper Cretaceous (~72 Ma), with the crown group established since the Paleocene (~58 Ma; see F1 + F2 strategy). This set of dates, largely congruent to recent divergence estimates, also suggest dispersal to be a primary driver of the anole biogeography in the Caribbean.

We also found that estimated ages in deep nodes are more prone to vary between chronograms than the ages of shallow nodes. Additionally, probably caused by sequence saturation, rate–based estimates strongly influenced deeper nodes by pulling these towards younger ages. The comparative approach used here also points out that the combination of fossil evidences outperforms the use of single calibration sources (e.g. F1 + F2 vs F1 or F2 in isolation). Furthermore, our analyses suggested that while deep–fossil calibrations resulted in smaller HPD across the tree, shallow fossil constraints produced wider ranges in divergence dates across the phylogeny.

Overall, we found that despite of the selected chronogram, Malpelo anole diverged at least 5 Ma before the island emergence. This mainly supports our previous findings that suggested small between–chronogram variance in shallow nodes. Moreover, the estimated timing suggests *A. agassizi* colonized the island from mainland (probably Central America where the sister clade is distributed).

Based on our analyses, we recommend further studies using molecular rates to estimate divergence dates to first test for sequence saturation in the analyzed dataset. Special caution should be taken when divergence dating analyses are focused on deep nodes (e.g. crown or stem groups) and are also exclusively based on molecular rates. This approach tends to sub-estimate the ages at the same nodes, but has minor effects on shallower nodes (e.g., divergence times between sister species). Finally, our study points out the importance of using of multiple node constraints, especially placed deeply in the phylogeny, when divergence dating analyses are exclusively based on fossil evidences. This latter approach specifically reduces the variation in estimated ages

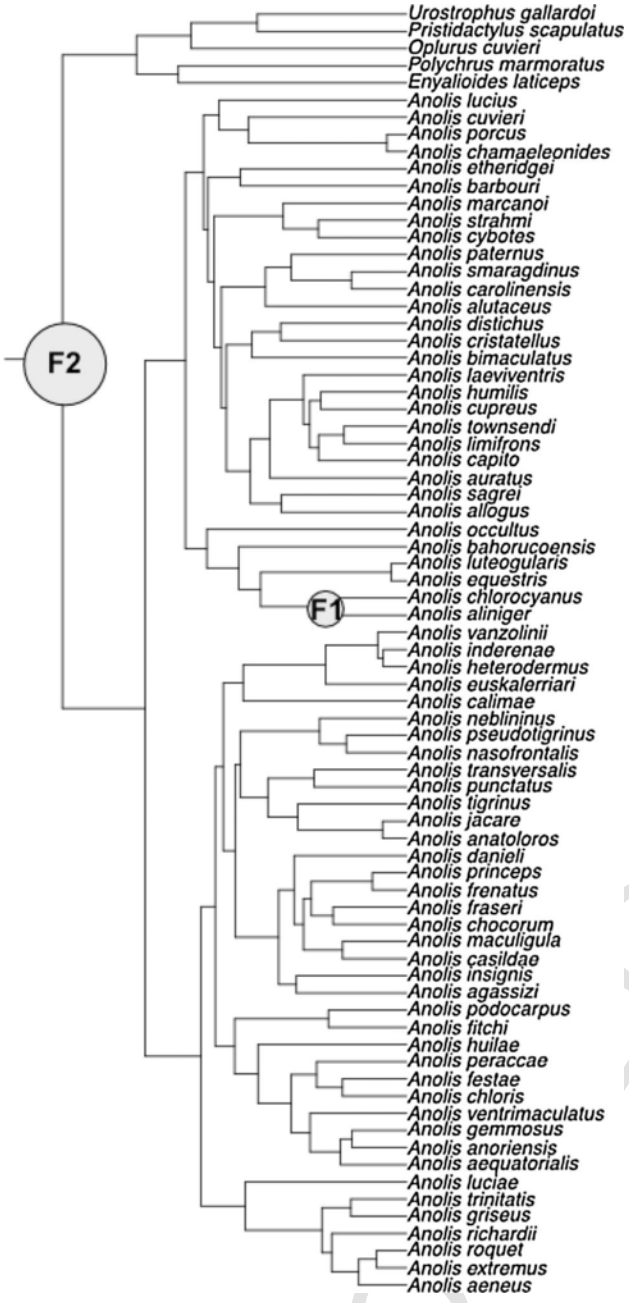

Fig. A1. Fossil constraints used in this study. Codes following information shown in Table 1.

across the phylogeny, and tends to also reduce the explicit bias intrinsic to single evidences.

Acknowledgements

CRP thanks the University of Arizona for financial support to work on this project. Colciencias and Universidad del Valle supported MdRC through the *Es Tiempo de Volver* fellowship (Convocatoria 656 – Resolución 0851, respectively). We also thank Kevin de Queiroz (National Museum of Natural History, Smithsonian Institution), Elizabeth Miller (University of Arizona), Mateo López-Victoria (Universidad Javeriana, Colombia), and Alejandro Valencia-Zuleta (Universidade Federal de Goiás, Brazil) for comments and discussion.

Appendix A.

See Figs. A1–A4 and Tables A1 and A2.

Appendix B. Supplementary material

Supplementary data associated with this article can be found, in the online version, at https://doi.org/10.1016/j.ympev.2018.06.012.

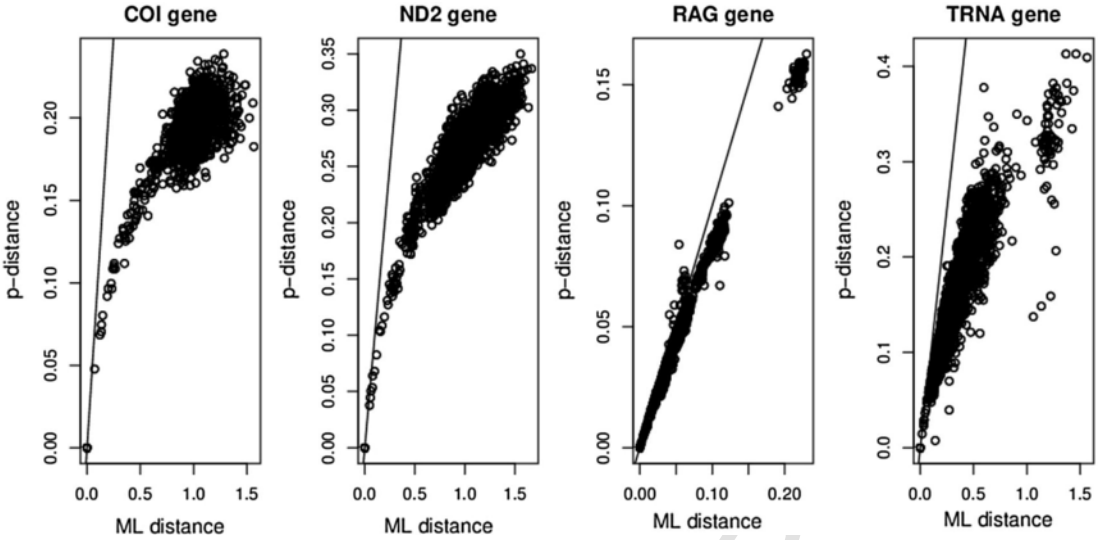

Fig. A2. Saturation plots for each gene regions (COI, ND2, RAG1, and tRNA). We plotted the uncorrected distances (p-distance) against corrected distances (ML distance) under HKY model. Non-saturated gene regions are expected to show a linear trend between the two distances and line curving is evidence of sequence saturation.

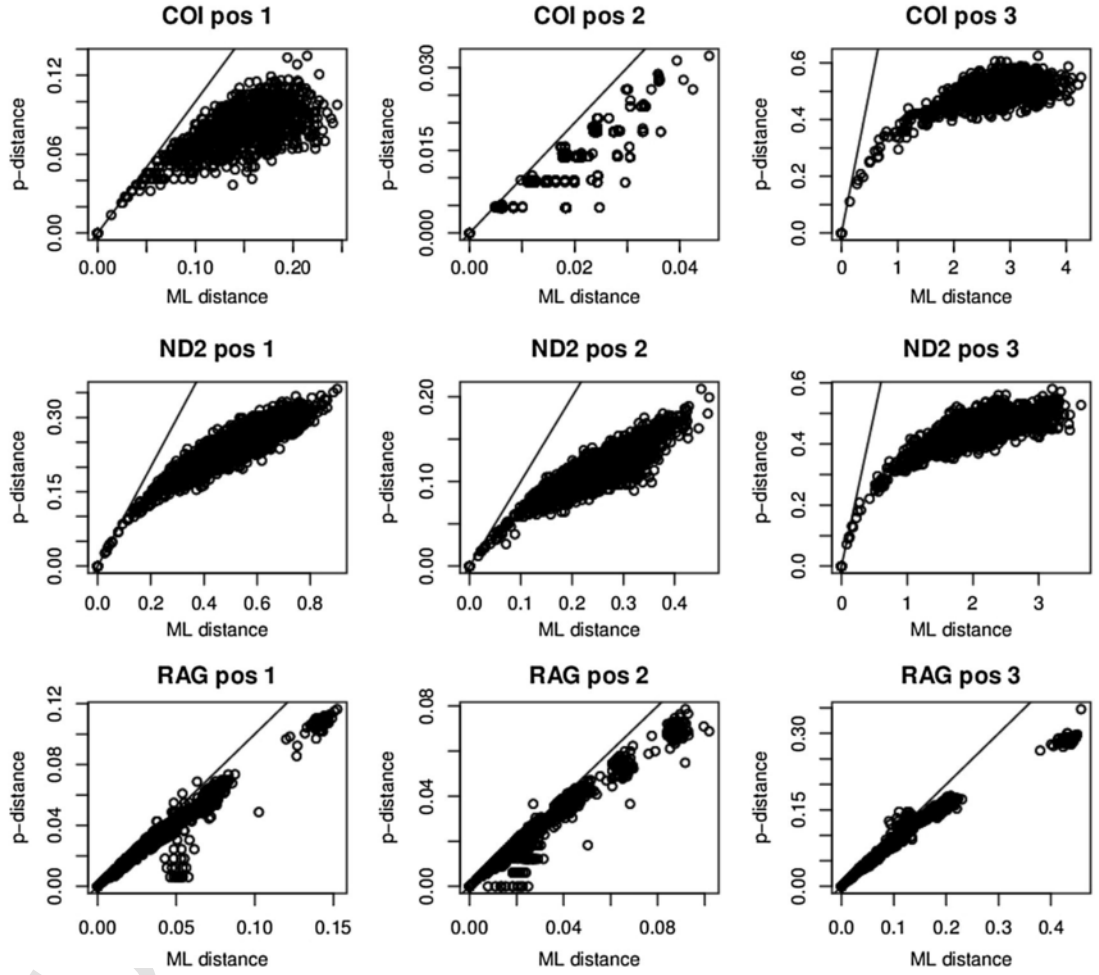

Fig. A3. Saturation plots for codon positions in each protein-coding gene (COI, ND2, RAG1). We plotted the uncorrected distances (p-distance) against corrected distances (ML distance) under HKY model. Non-saturated gene regions are expected to show a linear trend between the two distances and line curving is evidence of sequence saturation.

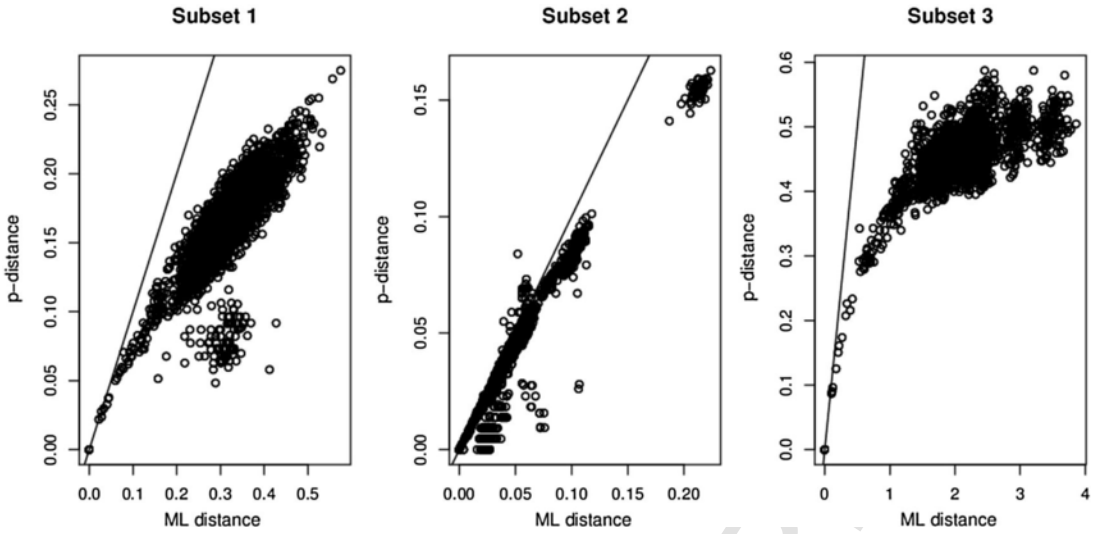

Fig. A4. Saturation plots for the partitions indicated by the best-fitting partitioning scheme (see Table A.2). We plotted the uncorrected distances (p-distance) against corrected distances (ML distance) under HKY model. Non-saturated gene regions are expected to show a linear trend between the two distances and line curving is evidence of sequence saturation.

Table A1
Summary of the sampled species used in this paper. GenBank accession number is provided for the three analyzed gene regions (COI, ND2 + tRNA, and RAG1).

Family	Species	Accession Number		
		COI	ND2 + tRNA	RAG1
Dactyloidae	*Anolis aeneus*	JN112719	AF055950	JN112592
	Anolis aequatorialis	JN112720	JN112662	JN112594
	Anolis agassizi	JN112722	JN112667	JN112595
	Anolis allogus	–	AY296152	Submitted
	Anolis alutaceus	–	AF055971	Submitted
	Anolis anatoloros	JN112723	JN112668	JN112596
	Anolis anoriensis	JN112734	JN112666	JN112609
	Anolis auratus	–	DQ377349	Submitted
	Anolis aligner	–	EF531485	KU979390
	Anolis bahorucoensis	–	AF055932	Submitted
	Anolis barbouri	–	AF055946	Submitted
	Anolis bimaculatus	JN112781	KF819777	JN112650
	Anolis calimae	JN112724	JN112670	JN112597
	Anolis capito	–	AY909744	Submitted
	Anolis carolinensis	–	AB473620	Submitted
	Anolis casildae	JN112726	AY909745	JN112599
	Anolis chamaeleonides	–	AF055975	Submitted
	Anolis chloris	JN112727	JN112671	JN112600
	Anolis chlorocyanus	–	EF531524	Submitted
	Anolis chocorum	JN112730	JN112674	JN112603
	Anolis cristatellus	–	AF055927	Submitted
	Anolis cupreus	JN112782	JN112717	JN112651
	Anolis cuvieri	JN112783	AF055973	JN112652
	Anolis cybotes	–	KC981478	Submitted
	Anolis danieli	JN112733	JN112676	JN112606
	Anolis distichus	–	GU734983	Submitted
	Anolis equestris	JN112784	EU107892	JN112653
	Anolis etheridgei	–	AF055934	Submitted
	Anolis euskalerriari	JN112737	JN112679	JN112611
	Anolis extremus	JN112739	AF317065	JN112612
	Anolis festae	JN112740	JN112680	JN112613
	Anolis fitchi	JN112741	JN112681	JN112615
	Anolis fraseri	JN112744	JN112684	JN112616
	Anolis frenatus	JN112746	JN112685	JN112619
	Anolis gemmosus	JN112747	JN112686	JN112621
	Anolis griseus	JN112749	AY296176	JN112622
	Anolis heterodermus	JN112751	JN112688	JN112624
	Anolis huilae	JN112754	JN112691	JN112627
	Anolis humilis	–	KJ953939	Submitted
	Anolis inderenae	JN112755	AY296145	JN112628
	Anolis insignis	JN112756	JN112693	–
	Anolis jacare	JN112759	JN112696	JN112630
	Anolis laeviventris	–	AY909756	Submitted
	Anolis limifrons	–	AF055943	Submitted
	Anolis luciae	JN112760	JN112697	JN112631
	Anolis lucius	JN112785	AF055962	JN112654
	Anolis luteogularis	–	AF055977	Submitted
	Anolis maculigula	JN112761	JN112698	JN112633
	Anolis marcanoi	JN112786	AF055955	JN112655
	Anolis neblininus	JN112763	JN112700	JN112634
	Anolis occultus	JN112787	AF055976	JN112656
	Anolis paternus	–	AF055965	Submitted
	Anolis peraccae	JN112764	JN112702	JN112636
	Anolis podocarpus	JN112780	JN112703	–
	Anolis porcus	–	AY296147	Submitted
	Anolis princeps	JN112768	JN112706	JN112639
	Anolis punctatus	JN112769	JN112707	JN112640
	Anolis richardii	JN112770	JN112708	JN112641
	Anolis roquet	JN112771	JN112709	JN112642
	Anolis sagrei	–	AB713054	JN112657
	Anolis smaragdinus	JN112788	JN112718	JN112658
	Anolis strahmi	–	AF055956	AF055956.2
	Anolis tigrinus	JN112772	JN112710	JN112643
	Anolis towsendi	–	KJ953922	KJ953922.1
	Anolis transversalis	JN112773	JN112711	JN112644
	Anolis trinitatis	JN112774	AY296204	JN112645
	Anolis vanzolinii	JN112775	JN112712	–
	Anolis ventrimaculatus	JN112777	JN112714	JN112646
Agamidae	*Agama agama*	–	AF128504	EU402825
	Leiolepis belliana	–	U82689	FJ356734
Chamaeleonidae	*Chamaeleo calyptratus*	–	AF448744	HQ876433
Hoplocercidae	*Enyalioides laticeps*	–	AF528719	EU586773

Table A1 (*Continued*)

Family	Species	Accession Number		
		COI	ND2 + tRNA	RAG1
Leiosauridae	*Pristidactylus scapulatus*	JN112790	–	JN112660
	Urostrophus gallardoi	JN112791	JN112703	JN112661
Opluridae	*Oplurus cuvieri*	–	U82685	JQ073188
Polychrotidae	*Polychrus marmoratus*	JN112789	–	JN112659

Table A2
Summary results for PartitionFinder analyses. Analyses were performed by including partitions based on codon positions for protein coding genes. The concatenated alignment (COI, ND2, RAG1, and tRNA genes) is provided in Supplementary File 1. We used BIC criteria and set the default parameters for PartitionFinder.

Parameter	Value
Scheme lnL	−75622.70625
Subset 1 (GTR + I + G)	COI position 1, ND2 position 1, ND2 position 2, tRNA
Subset 2 (GTR + I + G)	COI position 2, RAG1 position 1, RAG1 position 2, RAG1 position 3
Subset 3 (GTR + G)	COI position 3, ND2 position 3

References

Algar, A.C., Mahler, D.L., Ricklefs, R., 2016. Area, climate heterogeneity, and the response of climate niches to ecological opportunity in island radiations of Anolis lizards. Glob. Ecol. Biogeogr. 25, 781–791.

Andújar, C., Soria-Carrasco, V., Serrano, J., Gómez-Zurita, J., 2014. Congruence test of molecular clock calibration hypotheses based on Bayes factor comparisons. Methods Ecol. Evol. 5, 226–242.

Bessudo, S., Soler, G.A., Klimley, A.P., Ketchum, J.T., Hearn, A., Arauz, R., 2011. Residency of the scalloped hammerhead shark (Sphyrna lewini) at Malpelo Island and evidence of migration to other islands in the Eastern Tropical Pacific. Env. Biol. Fish. 91, 165–176.

Blankers, T., Townsend, T.M., Pepe, K., Reeder, T.W., Wiens, J.J., 2012. Contrasting global-scale evolutionary radiations: phylogeny, diversification, and morphological evolution in the major clades of iguanian lizards. Biol. J. Linn. Soc. 108, 127–143.

Bouckaert, R., Heled, J., Kühnert, D., Vaughan, T., Wu, C.-H., Xie, D., Suchard, M.A., Rambaut, A., Drummond, A.J., 2014. BEAST 2: A software platform for Bayesian evolutionary analysis. PLoS Comput. Biol. 10, e1003537.

Calsbeek, R., Smith, T.B., 2003. Ocean currents mediate evolution in island lizards. Nature 426, 552–555.

Campbell-Staton, S.C., Goodman, R.M., Backström, N., Edwards, S.V., Losos, J.B., Kolbe, J.J., 2012. Out of Florida: mtDNA reveals patterns of migration and pleistocene range expansion of the green anole lizard (Anolis carolinensis). Ecol. Evol. 2, 2274–2284.

Castañeda, M.d.R., de Queiroz, K., 2011. Phylogenetic relationships of the Dactyloa clade of Anolis lizards based on nuclear and mitochondrial DNA sequence data. Mol. Phylogenet. Evol. 61, 784–800.

Castañeda, M.d.R., Sherratt, E., Losos, J.B., 2014. The Mexican amber anole, Anolis electrum, within a phylogenetic context: implications for the origins of Caribbean anoles. Zool. J. Linn. Soc. 172, 133–144.

Conrad, J.L., 2008. Phylogeny and systematics of squamata (Reptilia) based on morphology. Bull. Am. Mus. Nat. Hist. 310, 1–182.

Crother, B., Guyer, C., 1996. Caribbean historical biogeography: was the dispersal-vicariance debate eliminated by an extraterrestrial bolide?. Herpetologica 52, 440–465.

Daza, J.D., Abdala, V., Arias, J.S., García-López, D., Ortiz, P., 2012. Cladistic analysis of Iguania and a fossil lizard from the Late Pliocene of Northwestern Argentina. J. Herpetol. 46, 104–119.

de Queiroz, K., Chu, L.-R., Losos, J.B., 1998. A second Anolis lizard in Dominican amber and the systematics and ecological morphology of Dominican amber anoles. Am. Museum Novitates 3249, 1–23.

Duchêne, S., Lanfear, R., Ho, S.Y., 2014. The impact of calibration and clock-model choice on molecular estimates of divergence times. Mol. Phylogenetics Evolut. 78, 277–289.

Edgar, R.C.R., 2004. MUSCLE: a multiple sequence alignment method with reduced time and space complexity. BMC Bioinf. 5, 113.

Fedorov, A.V., Dekens, P.S., McCarthy, M., Ravelo, A.C., Barreiro, M., Pacanowski, R.C., Philander, S.G., 2006. The Pliocene paradox (mechanisms for a permanent El Niño). Science 312, 1485–1489.

Guyer, C., Savage, J.M., 1986. Cladistic relationships among anoles (Sauria: Iguanidae). Syst. Zool. 35, 509–531.

Hartley, A.J., Chong, G., Houston, J., Mather, A.E., 2005. 150 million years of climate stability: Evidence from the Atacama Desert, northern Chile. J. Geol. Soc. 162, 421–444.

Hedges, S., 1996. Vicariance and dispersal in Caribbean biogeography. Herpetologica 52, 466–473.

Hedges, S.B., Hass, C.A., Maxson, L.R., 1992. Caribbean biogeography: molecular evidence for dispersal in West Indian terrestrial vertebrates. Proc. Natl. Acad. Sci. USA 89, 1909–1913.

Hedges, S., Hass, C., Maxson, L., 1994. Reply: towards a biogeography of the Caribbean. Cladistics 10, 43–55.

Hoernle, K., van den Bogaard, P., Werner, R., 2002. Missing history (16–71 Ma) of the Galápagos hotspot: implications for the tectonic and biological evolution of the Americas. Geology 30, 795–798.

Huber, M., Caballero, R., 2003. Eocene El Nino: Evidence for robust tropical dynamics in the "hothouse". Science 299, 877–881.

Jackman, T.R., Larson, A., de Queiroz, K., Losos, J.B., 1999. Phylogenetic relationships and tempo of early diversification in Anolis lizards. Syst. Biol. 48, 254–285.

Jiménez, L., Acosta, A., Chong, N., 2016. Population structure of Megabalanus peninsularis in Malpelo Island. Colombia. Rev. Biol. Trop. 51, 461–468.

Kass, R.E, Raftery, A.E. Bayes factors. 1995. J. Am. Stat. Assoc. 90, 773–95.

Kolbe, J.J., Revell, L.J., Szekely, B., Brodie, E.D., Losos, J.B., 2011. Convergent evolution of phenotypic integration and its alignment with morphological diversification in Caribbean Anolis ecomorphs. Evolution 65, 3608–3624.

Kumazawa, Y., Nishida, M., 1993. Sequence evolution of mitochondrial tRNA genes and deep-branch animal phylogenetics. J. Mol. Evol. 37, 380–398.

Lanfear, R., Calcott, B., Ho, S.Y.W., Guindon, S., 2012. Partitionfinder: combined selection of partitioning schemes and substitution models for phylogenetic analyses. Mol. Biol. Evol. 29, 1695–1701.

Macey, J.R., Schulte II, J.A., Ananjeva, N.B., Larson, A., Rastegar-Pouyani, N., Shammakov, S.M., Papenfuss, T.J., 1998. Phylogenetic relationships among agamid lizards of the Laudakia caucasia species group: testing hypotheses of biogeographic fragmentation and an area cladogram for the Iranian plateau. Mol. Phylogenet. Evol. 10, 118–131.

Macey, J.R., Schulte II, J.A., Larson, A., Tuniyev, B.S., Orlov, N., Papenfuss, T.J., 1999. Molecular phylogenetics, tRNA evolution, and historical biogeography in anguid lizards and related taxonomic families. Mol. Phylogenet. Evol. 12, 250–272.

Magallón, S., Hilu, K.W., Quandt, D., 2013. Land plant evolutionary timeline: gene effects are secondary to fossil constraints in relaxed clock estimation of age and substitution rates. Am. J. Bot. 100, 556–573.

Mahler, D.L., Ingram, T., Revell, L.J., Losos, J.B., 2013. Exceptional convergence on the macroevolutionary landscape in island lizard radiations. Science 341, 292–295.

Marshall, D.C., Hill, K.B., Moulds, M., Vanderpool, D., Cooley, J.R., Mohagan, A.B., Simon, C., 2016. Inflation of molecular clock rates and dates: molecular phylogenetics, biogeography, and diversification of a global cicada radiation from Australasia (Hemiptera: Cicadidae: Cicadettini). Sys. Biol. 65, 16–34.

Mello, B., Schrago, C.G., 2014. Assignment of calibration information to deeper phylogenetic nodes is more effective in obtaining precise and accurate divergence time estimates. Evol. Bioinforma. 10, 79–85.

Miller, M., Pfeiffer, W., Schwartz, T., 2011. The CIPRES science gateway: a community resource for phylogenetic analyses. P. 41. In: Proceedings of the 2011 TeraGrid Conference: extreme digital discovery.

Morey, R.D., Rouder, J.N., Jamil, T., 2015. BayesFactor: Computation of Bayes factors for common designs. R package version 0.9.

Mulcahy, D.G., Noonan, B.P., Moss, T., Townsend, T.M., Reeder, T.W., Sites Jr., J.W., Wiens, J.J., 2012. Estimating divergence dates and evaluating dating methods using phylogenomic and mitochondrial data in squamate reptiles. Mol. Phylogenet. Evol. 65, 974–991.

Nicholson, K.E., Crother, B.I., Guyer, C., Savage, J.M., 2012. It is time for a new classification of anoles (Squamata: Dactyloidae). Zootaxa 3477, 1–108.

O'Connor, M., Bruno, J., Gaines, S., 2007. Temperature control of larval dispersal and the implications for marine ecology, evolution, and conservation. Proc. Natl. Acad. Sci. USA 104, 1266–1271.

Phillips, M.J., 2009. Branch-length estimation bias misleads molecular dating for a vertebrate mitochondrial phylogeny. Gene 441, 132–140.

Poe, S., Nieto-Montes, D.O.A., Torres-Carvajal, O., de Queiroz, K., Velasco, J.A., Truett, B., Gray, L.N., Ryan, M.J., Köhler, G., Ayala-Varela, F., Latella, I., 2017. A phylogenetic, biogeographic, and taxonomic study of all extant species of Anolis (Squamata; Iguanidae). System. Biol. 66, 663–697.

Prates, I., Rodrigues, M.T., Melo-Sampaio, P.R., Carnaval, A.C., 2015. Phylogenetic relationships of Amazonian anole lizards (Dactyloa): taxonomic implications, new insights about phenotypic evolution and the timing of diversification. Mol. Phylogenet. Evol. 82, 258–268.

Rambaut, A., Suchard, M. A., Xie, D., Drummond. A., 2007. Tracer v1.6. <http://tree.bio.ed.ac.uk/software/tracer/>.

Rouder, J.N., Speckman, P.L., Sun, D., Morey, R.D., Iverson, G., 2009. Bayesian t-tests for accepting and rejecting the null hypothesis. Psychon. Bull. Rev. 16, 225–237.

Schwartz, R., Mueller, R., 2010. Branch length estimation and divergence dating: estimates of error in Bayesian and maximum likelihood frameworks. BMC Evol. Biol. 10, 5.

Sherratt, E., Castañeda, M.d.R., Garwood, R.J., Mahler, D.L., Sanger, T.J., Herrel, A., de Queiroz, K., Losos, J.B., 2015. Amber fossils demonstrate deep-time stability of Caribbean lizard communities. Proc. Natl. Acad. Sci. USA 112, 9961–9966.

Townsend, T.M., Mulcahy, D.G., Noonan, B.P., Sites, J.W., Kuczynski, C.A., Wiens, J.J., Reeder, T.W., 2011. Phylogeny of iguanian lizards inferred from 29 nuclear loci, and a comparison of concatenated and species-tree approaches for an ancient, rapid radiation. Mol. Phylogenet. Evol. 61, 363–380.

Uetz, P., Hošek, J., 2016. Amphisbaenians. The Reptile Database. Available at: <http://www.reptile-database.org> Accessed on 6 November 2016.

van Tuinen, C.R.T.M., 2015. Potential for bias and low precision in molecular divergence time estimation of the Canopy of Life: an example from aquatic bird families. Front. Genet. 6, 707.

Weir, J., Schluter, D., 2008. Calibrating the avian molecular clock. Mol. Ecol. 17, 2321–2328.

Wilke, T., Schultheiß, R., Albrecht, C., 2009. As time goes by: a simple fool's guide to molecular clock approaches in invertebrates. Am. Malacol. Bull. 27, 25–45.

Williams, E.E., 1976. West Indian anoles: a taxonomic and evolutionary summary. I Introduction and a species list. Breviora 440, 1–21.

Williams, E.E., 1976. South American anoles: the species groups. Papeis Avulsos Zool S. Paulo 29, 259–268.

Zheng, Y., Peng, R., Kuro-o, M., Zeng, X., 2011. Exploring patterns and extent of bias in estimating divergence time from mitochondrial DNA sequence data in a particular lineage: a case study of salamanders (Order Caudata). Mol. Biol. Evol. 28, 2521–2535.